Original Article

Investigating the optimal timing for the ultrasound prediction of a pathologic complete response in neoadjuvant breast cancer treatment

Jingwen Deng[1#], Shichong Liao[1#], Lijun Wang[1#], Jingwen Zhang[1,2], Yan Jia[3], Feng Yao[1], Shengrong Sun[1], Yimin Zhang[1]

[1]Department of Breast and Thyroid Surgery, Renmin Hospital of Wuhan University, Wuhan, China; [2]Center for Medical Ultrasound, The Affiliated Suzhou Hospital of Nanjing Medical University, Suzhou, China; [3]Department of Ultrasonography, Renmin Hospital of Wuhan University, Wuhan, China

Contributions: (I) Conception and design: Y Zhang; (II) Administrative support: S Sun, F Yao; (III) Provision of study materials or patients: S Liao, L Wang; (IV) Collection and assembly of data: J Deng, J Zhang, Y Jia; (V) Data analysis and interpretation: J Deng; (VI) Manuscript writing: All authors; (VII) Final approval of manuscript: All authors.

[#]These authors contributed equally to this work.

Correspondence to: Yimin Zhang, MD, PhD; Shengrong Sun, MD, PhD; Feng Yao, MD, PhD. Department of Breast and Thyroid Surgery, Renmin Hospital of Wuhan University, 238 Jiefang Road, Wuhan 430060, China. Email: dryiminzhang@163.com; sun137@sina.com; yaofengrmh@163.com.

Background: Neoadjuvant therapy (NAT) for breast cancer requires effective monitoring to assess the treatment response. To optimize treatment strategies, the early prediction of the therapeutic response is crucial. This study evaluated the predictive performance of three ultrasound models—the longest axis model (LAM), the dual axes model (DAM), and the manual segment model (MSM)—with a focus on early treatment cycles, and the relationship between tumor shrinkage and the probability of a pathologic complete response (pCR).

Methods: In total, 121 breast cancer patients (with 942 ultrasound images) at the Renmin Hospital of Wuhan University from December 2020 to July 2023 were enrolled in this prospective study. The ability of the three ultrasound models to predict the pCR across 6–8 NAT cycles was compared. Tumor response was measured as the tumor shrinkage ratio (TSR) relative to the baseline and the preceding cycle. Area under the curve (AUC) values were calculated for each model and cycle, and statistical significance was determined using the DeLong test. A logistic regression model based on the first-cycle MSM was used to quantify the relationship between the TSR and the probability of a pCR.

Results: The models had the highest AUC values in the first cycle of NAT, indicating their superior early predictive performance ($P<0.05$). Tumor shrinkage was significantly greater in the pCR group than in the non-pCR group. The logistic regression analysis based on the first-cycle MSM revealed a strong correlation between tumor shrinkage and the probability of a pCR, such that patients with ≥50% shrinkage had a higher likelihood of achieving a pCR.

Conclusions: Early cycle ultrasound assessments, particularly those that used the MSM, have strong predictive value for the pCR. Integrating a tumor shrinkage-based probability analysis enhances the predictive accuracy of the models. These findings support the use of early ultrasound evaluation in clinical practice to optimize NAT strategies and patient outcomes.

Keywords: Breast cancer; ultrasound; neoadjuvant therapy (NAT); pathologic complete response (pCR)

Submitted Jul 16, 2024. Accepted for publication Feb 27, 2025. Published online Mar 28, 2025.
doi: 10.21037/qims-24-1444
View this article at: https://dx.doi.org/10.21037/qims-24-1444

Introduction

Breast cancer continues to be one of the most prevalent oncological challenges worldwide, and represents a significant threat to women's health and mortality (1). Thus, sophisticated therapeutic strategies and robust evaluative methodologies need to be developed. Neoadjuvant therapy (NAT), which includes systemic chemotherapy and targeted therapy before surgical intervention, is the established protocol for the management of locally advanced breast cancer (2,3). This regimen is designed to downgrade the tumor stage, convert initially inoperable tumors into operable tumors, and augment the likelihood of breast-conserving procedures (4,5). The efficacy of NAT is typically gauged by monitoring dimensional reductions in the tumor across multiple treatment cycles (6-8).

The pathologic complete response (pCR), which is defined as the absence of invasive or non-invasive cancer remnants in breast and axillary pathology post-treatment (9), is a prognostic marker associated with improved survival outcomes (10,11). However, the accurate prediction of the pCR during NAT remains a clinical challenge. Traditional imaging techniques, such as mammography, magnetic resonance imaging (MRI), and breast ultrasound, are routinely used to assess patients undergoing NAT (12-14). Contrast-enhanced MRI is considered the most accurate method for detecting tumor responses to NAT (15,16); however, its high costs and relatively long examination time limit its frequent use. Mammography is particularly sensitive to calcifications; however, the relationship between calcific responses and therapeutic efficacy remains unclear, and some studies have reported that its performance in monitoring chemotherapeutic responses is suboptimal (17,18). Advanced breast examination technologies, such as digital breast tomosynthesis (19), automated whole-breast ultrasound (20), molecular breast imaging (21), and artificial intelligence–assisted diagnostic systems, are currently under investigation but are not yet widely used in clinical practice. Due to its real-time imaging capabilities and cost effectiveness, ultrasound stands out as a promising tool for monitoring the treatment response (22-25). By enabling the early prediction of the pCR through ultrasound, clinicians can customize treatment regimens to minimize the adverse effects of ineffective therapies and support more personalized therapeutic decision making. However, research on the optimal timing and frequency for ultrasound examinations during NAT is limited.

This study was designed to explore the optimal timing for ultrasound use in predicting the pCR in breast cancer patients undergoing NAT. Specifically, it investigated the ability of early treatment cycle ultrasound examinations to reliably predict treatment outcomes. A prospective study involving continuous ultrasound assessments of breast cancer patients undergoing NAT was conducted to collect clinical data to evaluate the effectiveness of various ultrasound measurement techniques. By assessing the predictive accuracy of ultrasound at different stages of NAT, this research aimed to strengthen clinical decision-making processes, ultimately enhancing patient prognoses and optimizing therapeutic outcomes. We present this article in accordance with the TRIPOD + AI reporting checklist (available at https://qims.amegroups.com/article/view/10.21037/qims-24-1444/rc).

Methods

Patients

This study prospectively collected 2,040 ultrasound images from 278 breast cancer patients at the Renmin Hospital of Wuhan University from December 2020 to July 2023. After a standardized selection process, 121 breast cancer patients with 942 ultrasound images were ultimately enrolled in the study. All the patients underwent pre-treatment breast core needle biopsy and were confirmed to have malignant breast tumors. All the patients completed the entire course of treatment, and underwent periodic breast ultrasound examinations, and surgical excision and pathological examination after treatment completion. Complete pathology reports were available for all the patients. *Figure 1* provides a schematic of the patient selection process. The study was conducted in accordance with the Declaration of Helsinki (as revised in 2013). The study was approved by the Ethics Committee of the Renmin Hospital of Wuhan University (approval No. WDRY2022-K217). All participants provided written informed consent for ultrasound examinations, surgical treatment, and the use of their data.

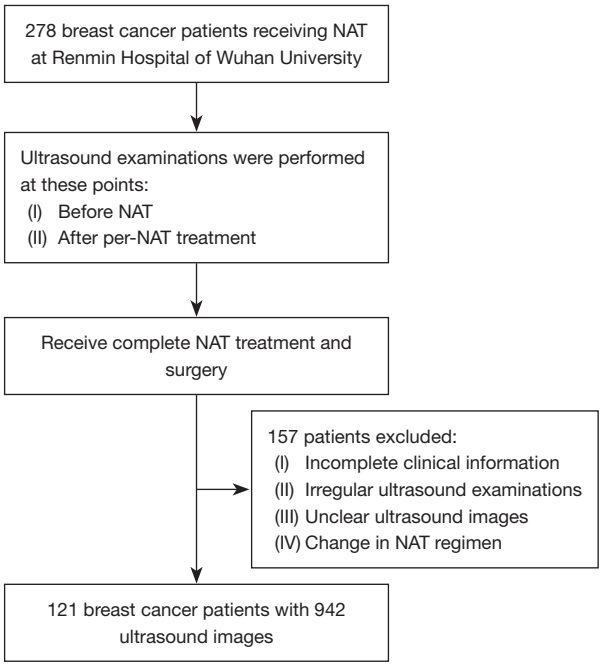

Figure 1 Patient selection and study flowchart. This chart displays the selection process for breast cancer patients undergoing NAT at the Renmin Hospital of Wuhan University. Ultrasound examinations were conducted before NAT and after each treatment cycle. In total, 278 patients were initially identified for inclusion in the study; however, 157 patients were excluded for reasons including incomplete clinical data, irregular ultrasound schedules, poor image quality, or changes in the NAT protocol. Ultimately, 121 patients (with 942 ultrasound images) who received complete NAT and surgery were included in the study. NAT, neoadjuvant therapy.

Inclusion criteria

To be eligible for inclusion in the study, the patients had to meet the following inclusion criteria: (I) have a pathologically confirmed diagnosis of primary invasive breast cancer via biopsy; (II) have not received breast cancer treatment, and have the following indications: a tumor size >5 cm; human epidermal growth factor receptor 2 (HER2)-positive status; and estrogen receptor (ER)-, progesterone receptor (PR)-, and HER2-negative status; axillary lymph node metastasis, or a strong intent for breast conservation; (III) have completed 6–8 cycles of NAT; (IV) have undergone breast ultrasound examinations before NAT and after each treatment cycle; and (V) have undergone surgical excision after the completion of NAT and a subsequent pathological examination.

Exclusion criteria

Patients were excluded from the study if they met any of the following exclusion criteria: (I) had changed their chemotherapy regimen partway through treatment; (II) had undergone surgical intervention before completing the full course of NAT; (III) had breast tumor ultrasound images that were not of sufficient quality for accurate assessment; and/or (IV) had incomplete pathological results following surgical excision.

Acquisition of ultrasound images and clinical information

The study implemented several measures to minimize operator dependency and ensure the consistency of the ultrasound measurements. First, patient examinations were conducted using the same ESAOTE MEGAS GPX FD570A (Esaote S.p.A., Genoa, Italy) ultrasound diagnostic device, with the probe set to a linear array and the frequency range adjusted to 5–13 MHz. All patients were placed in the supine or semi-lateral position (with a pillow of suitable height placed under the posterior axillary line for those with larger breasts), with their arms abducted to fully expose the breast. Second, the examinations followed a standardized imaging protocol based on the American College of Radiology's Breast Imaging Reporting and Data System, which included patient positioning, probe orientation, and measurement methods. All scans were performed by two experienced sonographers with 5–10 years of experience in breast ultrasound imaging each, and standardized workflows were adopted for image acquisition and reporting. For each patient, the two sonographers independently conducted the examinations, and only consistent findings were reported. Additionally, all measurement results were reviewed and verified by a specialist with over 10 years of experience in breast ultrasound diagnostics. The clinical data of the patients were collected from the institution's electronic health records system, including patient age, date of diagnosis, menopausal status, pathological type, ER status, PR status, HER2 status, Ki-67 index, and Residual Cancer Burden (RCB) index after surgery.

Neoadjuvant treatment regimen and efficacy evaluation

All patients underwent 6–8 complete cycles of NAT. The treatment protocols were based on the 2020–2023 National Comprehensive Cancer Network guidelines and the Chinese Society of Clinical Oncology guidelines for the diagnosis and treatment of breast cancer (26-29).

The most common treatment regimen for patients with triple-negative breast cancer is epirubicin, cyclophosphamide, and taxol, while the most common regimen for patients with HER2-positive tumors is taxol, carboplatin, trastuzumab, and pertuzumab, which are administered every 21 days. Following NAT, the surgically excised breast tumor tissues were sent to the Pathology Department where specialist pathologists examined the specimens. The RCB index (30) was used as the standard for evaluating the residual tumor after NAT in breast cancer. The pCR was defined as the complete absence of invasive cancer in the breast and axillary lymph nodes (31). The pathological evaluation and ultrasound assessment were conducted independently.

Measurement of tumor shrinkage

According to the Response Evaluation Criteria in Solid Tumors (RECIST, version 1.1) (32), tumor size was assessed by ultrasound after each cycle of NAT. For patients with multifocal disease, the tumor size was defined as the sum of the size of each tumor. The following three measurement methods were used to evaluate tumor shrinkage: the longest axis model (LAM), which takes the maximum value provided by the ultrasound report for the current cycle; the dual axes model (DAM), which is the product of the longest diameter and the perpendicular short diameter as reported in the ultrasound for that cycle; and the manual segment model (MSM), where experienced sonographers use 3D slicer (version 5.4.0) to annotate the tumor boundaries and area, and the area is automatically output by the software. *Figure 2* shows these measurement methods applied across multiple cycles, providing representative examples from both a pCR patient and a non-pCR patient.

Receiver operating characteristic (ROC) analysis and tumor shrinkage modeling

To evaluate the predictive performance of the three ultrasound-based tumor measurement models in predicting the pCR, ROC curves were constructed using the tumor shrinkage ratio (TSR) as the variable, and the area under the curve (AUC) values were calculated. ROC curves were generated for each NAT treatment cycle to assess the temporal predictive accuracy of each model. Pairwise AUC comparisons across cycles and models were conducted using the DeLong test. To further assess the longitudinal performance of these models, combined ROC curves were constructed by aggregating cycle-specific AUC values and visualized as step plots. In addition, a logistic regression model was used to analyze the relationship between the TSR in the first cycle measured by the MSM and the probability of achieving a pCR, and the results were presented as a predictive probability curve. All statistical analyses were performed using the "pROC" and "ggplot2" packages in R (version 4.3.2). The TSR was calculated using the following formula:

$$TSR = \frac{T_{c-1} - T_c}{T_{c-1}} \times 100\% \quad [1]$$

where T_{c-1} is the tumor size at the previous cycle, and T_c is the tumor size at the current cycle.

Statistical analysis

The statistical analyses were conducted using R (version 4.3.2). Data following a normal distribution are presented as mean ± standard deviation. Normality was tested using the Shapiro-Wilk test. For comparisons between two groups, the normally distributed data were analyzed using the *t*-test, while the non-normally distributed data were assessed using the Wilcoxon rank-sum test. For the categorical variables, differences between groups were determined using the Chi-squared test. Multiple group comparisons were conducted using the Kruskal-Wallis test. A P value <0.05 was considered statistically significant.

Results

Patient information

In this study, the data of 121 breast cancer patients undergoing NAT were analyzed to compare the characteristics of those who did not achieve a pCR (non-pCR) with those who did (pCR) (*Table 1*). The average age of the patients in the non-pCR group (47.26±9.79 years) was significantly lower than that of the patients in the pCR group (52.07±10.94 years), and the difference was statistically significant (P=0.012). Statistically significant differences were also observed between the two groups in terms of histological grading (P=0.001) and receptor status, including ER (P<0.001), PR (P<0.001), and HER2 (P<0.001) status. No significant differences were found between the two groups in terms of menopausal state (P=0.065), tumor type (P=0.222), N stage (P>0.999), T stage (P=0.785), and Ki-67 status (P=0.082).

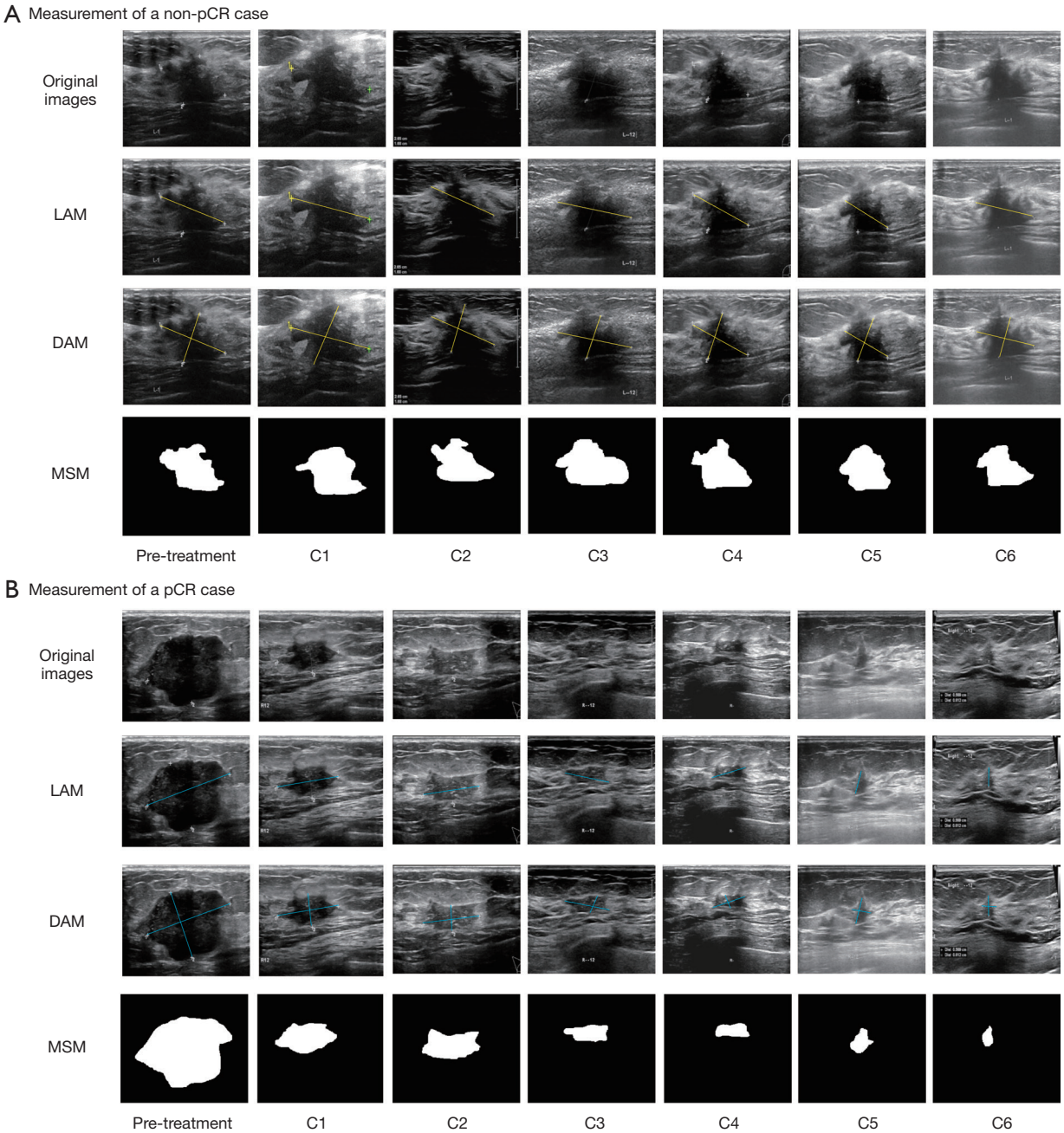

Figure 2 Representative tumor shrinkage across treatment cycles for non-pCR and pCR cases. This figure presents a series of representative ultrasound images from different cycles of NAT in breast cancer patients. It displays original images, followed by analyses using the LAM, DAM, and MSM. These sections illustrate changes in tumor measurements and segmentation across treatment cycles, demonstrating tumor shrinkage over time. (A) A non-pCR case: this panel displays a series of ultrasound images illustrating tumor shrinkage in a patient who did not achieve a pCR. (B) A pCR case: this panel displays a series of ultrasound images illustrating tumor shrinkage in a patient who achieved a pCR. C, treatment cycle; DAM, dual axes model; LAM, longest axis model; MSM, manual segment model; NAT, neoadjuvant therapy; pCR, pathologic complete response.

Table 1 Basic information

Characteristic	Patients (n=121)		P value
	Non-pCR (n=65)	pCR (n=56)	
Age (years)	47.26±9.79	52.07±10.94	0.012*
Menopausal state			0.065
Pre-menopausal	41 (63.08)	25 (44.64)	
Post-menopausal	24 (36.92)	31 (55.36)	
Tumor type			0.222
Invasive ductal carcinoma	35 (53.85)	23 (41.07)	
Other	30 (46.15)	33 (58.93)	
Histological grading			0.001*
Low-grade invasive breast cancer (WHO I, II)	28 (43.08)	8 (14.29)	
High-grade invasive breast cancer (WHO III)	37 (56.92)	48 (85.71)	
N stage			>0.999
0	23 (35.38)	20 (35.71)	
1–3	42 (64.62)	36 (64.29)	
T stage			0.785
1	12 (18.46)	8 (14.29)	
2	46 (70.77)	42 (75.00)	
3	7 (10.77)	6 (10.71)	
ER status			<0.001*
Positive	44 (67.69)	16 (28.57)	
Negative	21 (32.31)	40 (71.43)	
PR status			<0.001*
Positive	40 (61.54)	9 (16.07)	
Negative	25 (38.46)	47 (83.93)	
HER2 status			<0.001*
Positive	15 (23.08)	42 (75.00)	
Negative	50 (76.92)	14 (25.00)	
Ki-67 status			0.082
<20%	16 (24.62)	6 (10.71)	
≥20%	49 (75.38)	50 (89.29)	

Data were presented as mean ± standard deviation or n (%). *, P<0.05 was considered statistically significant. ER, estrogen receptor; HER2, human epidermal growth factor receptor 2; pCR, pathologic complete response; PR, progesterone receptor; WHO, World Health Organization.

Tumor shrinkage trends

Patients underwent breast ultrasound to assess tumor shrinkage after each cycle of NAT, and received surgical treatment after completing 6–8 cycles of NAT (21 days per cycle). *Figure 3* displays the tumor shrinkage trends and the distribution of individual patient NAT data using the three measurement methods; that is, the MSM (*Figure 3A*), LAM (*Figure 3B*), and DAM (*Figure 3C*). Each line graph differentiates between the pCR and non-pCR patients.

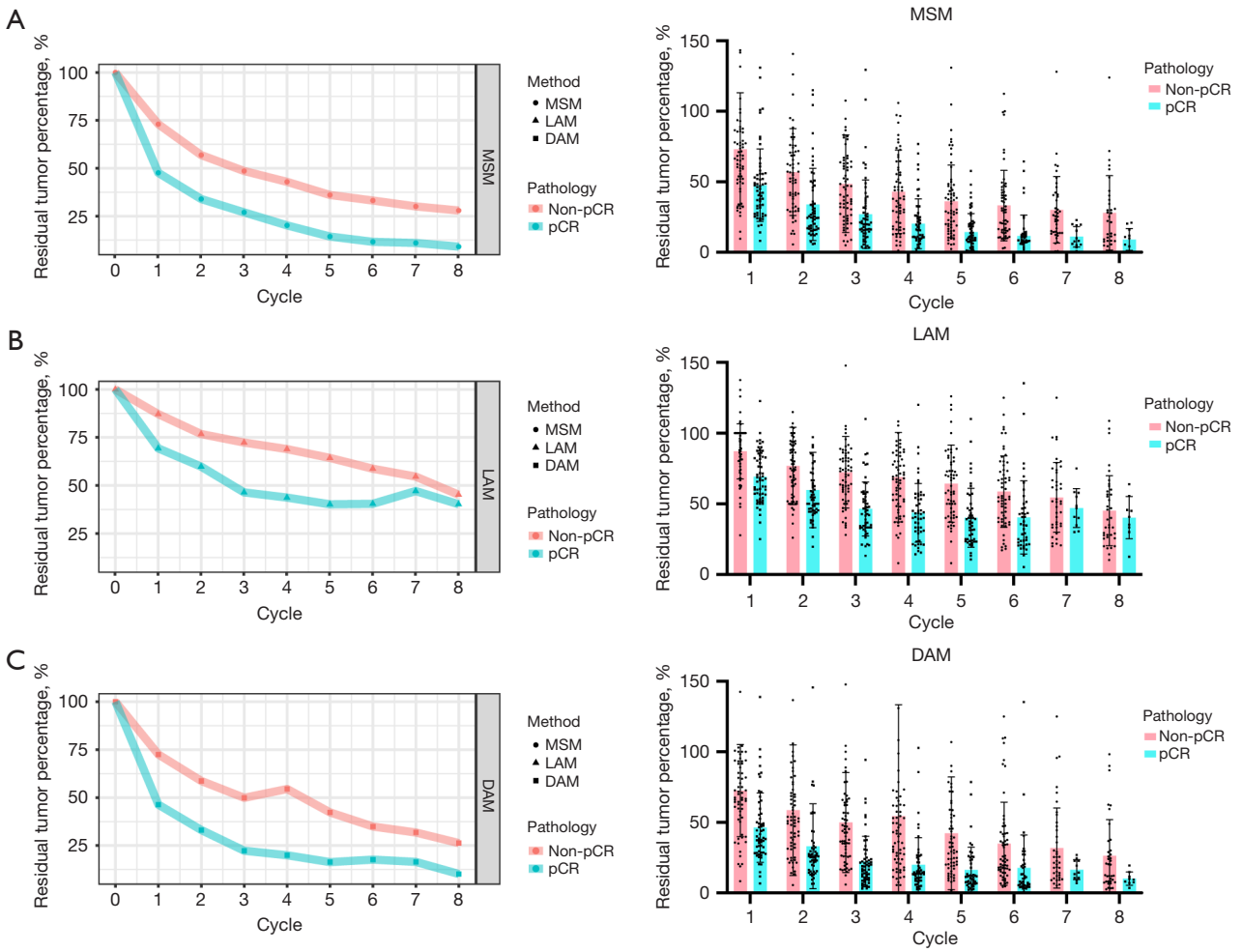

Figure 3 Comparative analysis of tumor shrinkage by ultrasound models and pathological response across NAT cycles. This figure illustrates the progression of residual tumor percentages as assessed by the three different ultrasound models. Each panel is divided into two parts: the left graph shows trend lines representing the average residual tumor percentage across 8 cycles of NAT for both the pCR and non-pCR groups; the right graph displays the distribution of individual patient residual tumor percentages for each cycle, categorized by pCR and non-pCR, with bars indicating median values, and error bars showing interquartile ranges. (A) Shrinkage trends and patient data assessed by the MSM. (B) Shrinkage trends and patient data assessed by the LAM. (C) Shrinkage trends and patient data assessed by the DAM. DAM, dual axes model; LAM, longest axis model; MSM, manual segment model; NAT, neoadjuvant therapy; pCR, pathologic complete response.

As the graphs show, while tumor shrinkage occurred in both groups, the reduction was more pronounced in the pCR group, which had a residual tumor size decrease to less than 50% of the original size after the first two cycles, compared to the non-pCR group, which maintained a residual tumor size greater than 50%. Notably, the MSM showed a more distinct early separation between the groups, highlighting its enhanced sensitivity in tracking early tumor shrinkage changes.

Ultrasound assessment of NAT efficacy across different cycles

To assess whether ultrasound could differentially predict the likelihood of achieving a pCR after completing NAT across different cycles, ROC curves for the three models were established (*Figure 4*). In the first cycle of NAT, the AUC values for the LAM, DAM, and MSM were the highest among all cycles at 0.764 [95% confidence interval (CI): 0.679–0.849], 0.756 (95% CI: 0.667–0.846), and 0.744 (95%

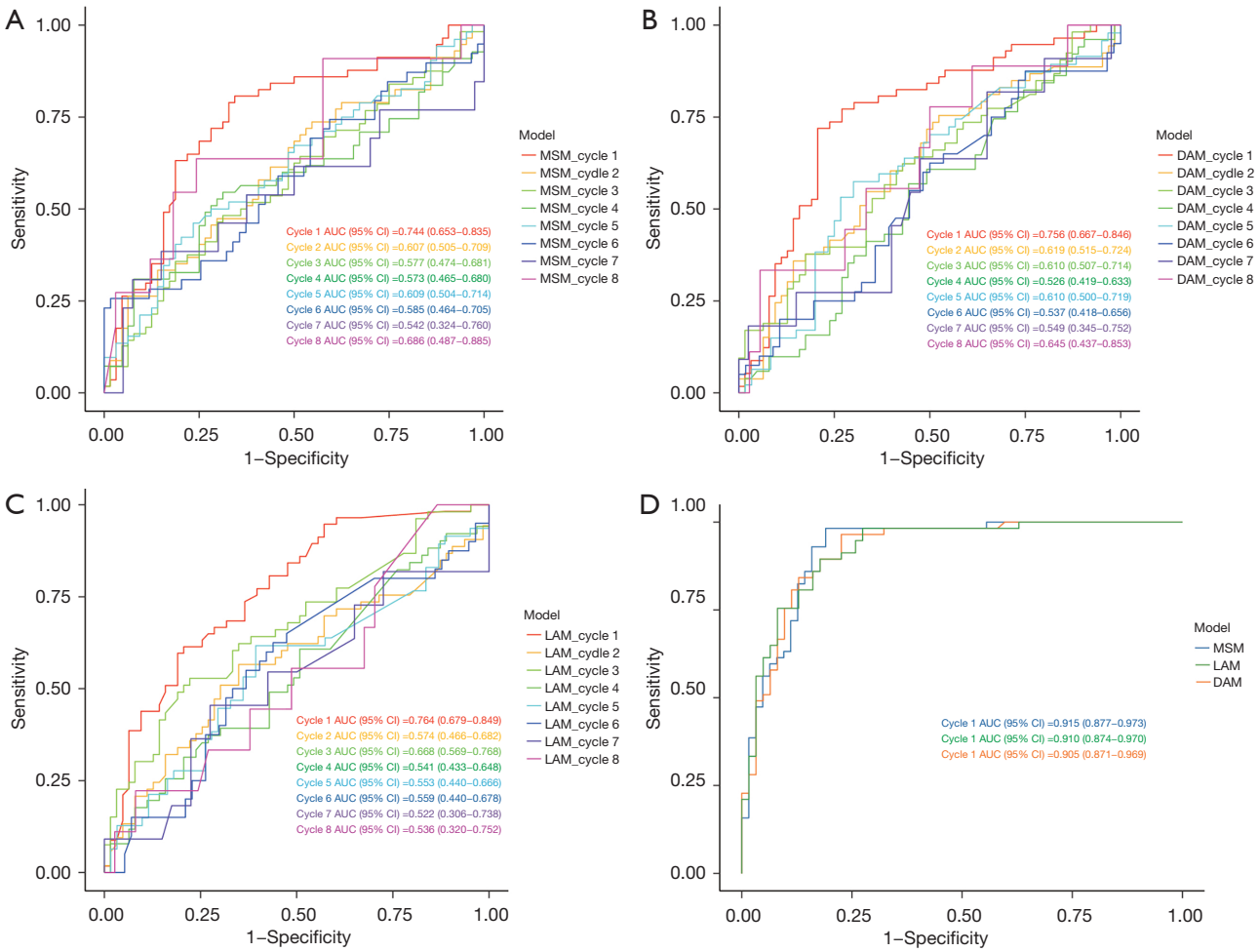

Figure 4 ROC curves for ultrasound models predicting the pCR across the NAT cycles, and the enhanced first-cycle analysis results. This figure displays the ROC curves that were used to evaluate the predictive performance of the three ultrasound models across all cycles of NAT. The AUC values for each cycle are annotated, and provide a measure of each model's diagnostic accuracy at different stages of treatment. (A) ROC curve and cycle-specific AUC values for the MSM. (B) ROC curve and cycle-specific AUC values for the DAM. (C) ROC curve and cycle-specific AUC values for the LAM. (D) The first-cycle ROC curves for all models after incorporating clinical and pathological features. AUC, area under the curve; CI, confidence interval; DAM, dual axes model; LAM, longest axis model; MSM, manual segment model; NAT, neoadjuvant therapy; ROC, receiver operating characteristic.

CI: 0.653–0.835), respectively. The AUCs were compared using the DeLong test (*Tables 2-4*), and differed significantly compared to other cycles (LAM: C1 *vs.* C2, C4, C5, C6, P<0.05; DAM: C1 *vs.* C3, C4, C6, P<0.05; MSM: C1 *vs.* C2, C3, C4, C6, C7, P<0.05). This indicates that the predictive efficacy of the DAM, MSM, and LAM was superior in the first cycle of NAT; thus, the first cycle is the most effective period for prediction. In addition, after incorporating common clinical and pathological indicators (i.e., age, menopausal status, pathological type, ER status, PR status, HER2 status, and the Ki-67 index), the ROC curves for the first cycle had significantly higher AUC values. *Figure 4D* compares these models in the first cycle after including clinical and pathological features, and shows an increase in AUC values (LAM from 0.764 to 0.910, DAM from 0.756 to 0.905, and MSM from 0.744 to 0.915), demonstrating an improvement in predictive ability. Thus, the ultrasound models achieved better predictive accuracy early on when integrated with clinical data.

Subsequently, we evaluated the effectiveness of the three tumor measurement models over eight cycles of NAT, using AUC values to gauge their discriminative ability (*Figure 5*).

Table 2 P values for all cycles of NAT using the LAM

Cycle	Cycle							
	1	2	3	4	5	6	7	8
1	–	0.008*	0.134	0.001*	0.006*	0.004*	0.134	0.577
2	0.008*	–	0.258	0.833	0.903	0.449	0.453	0.345
3	0.134	0.258	–	0.112	0.097	0.185	0.320	0.382
4	0.001*	0.833	0.112	–	0.948	0.998	0.844	0.913
5	0.006*	0.903	0.097	0.948	–	0.937	0.891	0.793
6	0.004*	0.449	0.185	0.998	0.937	–	0.991	0.854
7	0.134	0.453	0.320	0.844	0.891	0.991	–	0.669
8	0.577	0.345	0.382	0.913	0.793	0.854	0.669	–

*, P<0.05 was considered statistically significant. LAM, longest axis model; NAT, neoadjuvant therapy.

Table 3 P values for all cycles of NAT using the DAM

Cycle	Cycle							
	1	2	3	4	5	6	7	8
1	–	0.065	0.024*	0.001*	0.072	0.003*	0.247	0.879
2	0.065	–	0.921	0.358	0.701	0.888	0.884	0.483
3	0.024*	0.921	–	0.357	0.725	0.163	0.206	0.886
4	0.001*	0.358	0.357	–	0.474	0.989	0.951	0.650
5	0.072	0.701	0.725	0.474	–	0.376	0.879	0.435
6	0.003*	0.888	0.163	0.989	0.376	–	0.757	0.456
7	0.260	0.888	0.208	0.951	0.883	0.754	–	0.304
8	0.879	0.483	0.886	0.650	0.435	0.456	0.296	–

*, P<0.05 was considered statistically significant. DAM, dual axes model; NAT, neoadjuvant therapy.

Table 4 P values for all cycles of NAT using the MSM

Cycle	Cycle							
	1	2	3	4	5	6	7	8
1	–	0.049*	0.013*	0.029*	0.062	0.027*	0.035*	0.758
2	0.049*	–	0.779	0.777	0.787	0.650	0.186	0.880
3	0.013*	0.779	–	0.971	0.743	0.814	0.590	0.161
4	0.029*	0.777	0.971	–	0.417	0.690	0.749	0.714
5	0.062	0.787	0.743	0.417	–	0.927	0.698	0.167
6	0.027*	0.650	0.814	0.690	0.927	–	0.868	0.746
7	0.035*	0.186	0.590	0.749	0.698	0.868	–	0.251
8	0.758	0.880	0.161	0.714	0.167	0.746	0.251	–

*, P<0.05 was considered statistically significant. MSM, manual segment model; NAT, neoadjuvant therapy.

As *Figure 5* shows, the predictive ability of the three models across all NAT cycles was directly compared without adding additional factors to explicitly assess their diagnostic efficacy in a standardized setting. The AUC values and 95% CIs revealed that the performance of the models was closely matched in the early treatment cycles, but slight variations appeared as the therapy progressed. Notably, the statistical comparisons revealed few significant differences between the models (P>0.05), except in cycle 8 where a significant difference was observed between the LAM and MSM (P=0.046). Overall, the data suggest that all the models performed comparably in measuring tumor shrinkage.

After evaluating the ROC curve performance of specific cycles and models, the longitudinal predictive trends of the three ultrasound-based models were further examined by aggregating the AUC values across all NAT cycles (*Figure 6A-6C*). The step plots illustrate the temporal variations in predictive accuracy. Notably, the MSM exhibited a stable upward trend across cycles, with AUC values increasing from 0.744 to 0.909. Conversely, the DAM and LAM showed more pronounced fluctuations. The early cycle AUC values were consistently gradually increased across all models; however, later cycles exhibited greater variability, particularly in the LAM.

To quantitatively evaluate the relationship between tumor shrinkage and the likelihood of achieving a pCR, a logistic regression model was constructed using MSM-measured tumor shrinkage after the first NAT cycle (*Figure 6D*). The curve revealed a positive correlation between tumor shrinkage and the probability of achieving a pCR. Specifically, patients with 50% tumor shrinkage had a predicted probability of achieving a pCR of 51.9%. For patients with more than 70% tumor shrinkage (defined as a partial response by the RECIST), the probability of achieving a pCR reached 65.9% or higher. The calculation formula was expressed as follows:

$$P(pCR) = \frac{1}{1+\exp(1.372-0.029\times TSR)}\times 100\% \quad [2]$$

Discussion

In this study, three ultrasound models (i.e., the LAM, DAM, and MSM) were used to assess the scale of tumor shrinkage during NAT, and their predictive efficacy was compared across different treatment cycles. As a primary imaging modality, ultrasound offers significant advantages in monitoring tumor size and morphology dynamically. It is particularly effective in assessing residual size, detecting concentric shrinkage, and observing changes in internal echogenicity, all of which contribute to predicting the pCR (33). Among these, tumor size reduction is the most direct and reliable indicator of the treatment response (34).

The key finding of this study was that all three ultrasound models showed the highest predictive efficacy for the pCR in the first cycle of NAT. In the first cycle, tumor shrinkage was significantly greater in the pCR group than the non-pCR group (*Figure 3*), and the AUC values for all three models peaked (*Figure 4A-4C*). This suggests that the tumor response in the initial phase of treatment could serve as an early indicator of therapeutic efficacy. The predictive advantage of early cycle ultrasound assessments was further confirmed by the DeLong test, which revealed that the AUC values were significantly higher in the first cycle than most later cycles (P<0.05). Conversely, as treatment progressed, the predictive power of the ultrasound models decreased, with greater variability observed in later cycles, particularly for the LAM. The LAM, which relies on a single-axis measurement, may fail to capture complex tumor shrinkage patterns, particularly in cases of non-concentric shrinkage or irregular morphology.

To further quantify the relationship between early tumor shrinkage and the likelihood of pCR, we developed a logistic regression model based on first-cycle MSM tumor shrinkage (*Figure 6D*). The model revealed a strong positive correlation between tumor shrinkage and the probability of a pCR. Patients with significant shrinkage (>50%) in the first cycle were more likely to achieve a pCR (>50%). These findings provide a quantitative framework for early response–based patient stratification, reinforcing the clinical utility of first-cycle ultrasound in guiding treatment decisions.

Our findings align with those of previous studies emphasizing the role of ultrasound in NAT response monitoring. Lim *et al.* (23) showed that ultrasound-based changes in the longest tumor diameter significantly predict the RCB and pCR, with early reductions serving as strong indicators of the treatment response. Sabeti *et al.* (25) showed the value of early cycle ultrasound assessments, and found that incorporating quantitative high-definition microvasculature imaging enhanced monitoring precision in predicting the neoadjuvant chemotherapy response. Similarly, Duan *et al.* (35) developed a predictive model that integrated shear wave elastography and core needle biopsy pathology, and found significant associations between tumor elasticity parameters and Miller-Payne grading, as well as RCB classification (AUC: 0.855). Wen *et al.* (36) expanded on this by incorporating ultrasound morphological features

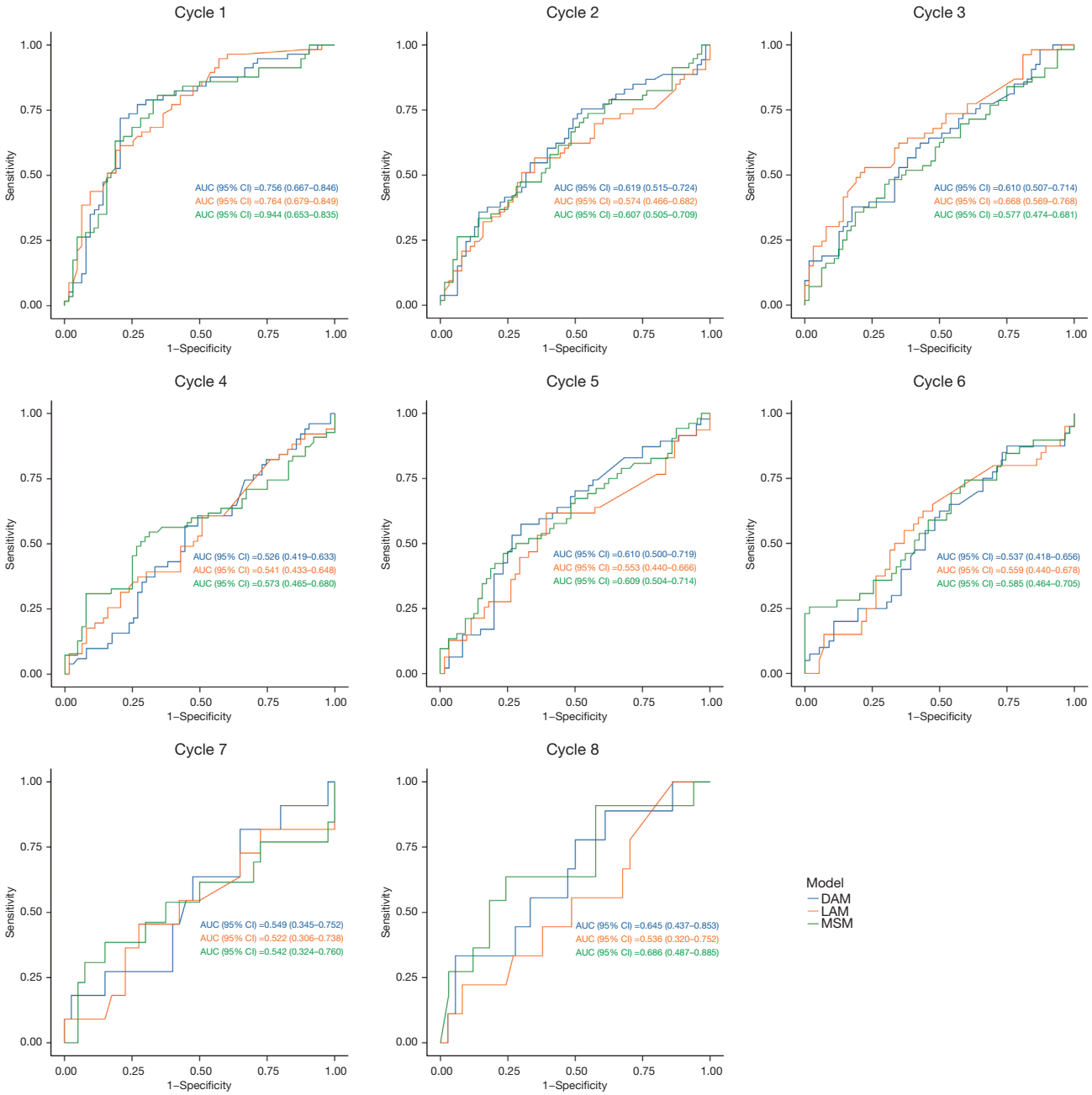

Figure 5 Comparative ROC curves for three ultrasound models across the NAT cycles. This figure shows the ROC curves for the three ultrasound models. Each curve shows the performance of the models in predicting pCR for each cycle of NAT. The AUC value for each curve quantifies the predictive accuracy of the model across the treatment cycles. AUC, area under the curve; CI, confidence interval; DAM, dual axes model; LAM, longest axis model; MSM, manual segment model; NAT, neoadjuvant therapy; ROC, receiver operating characteristic.

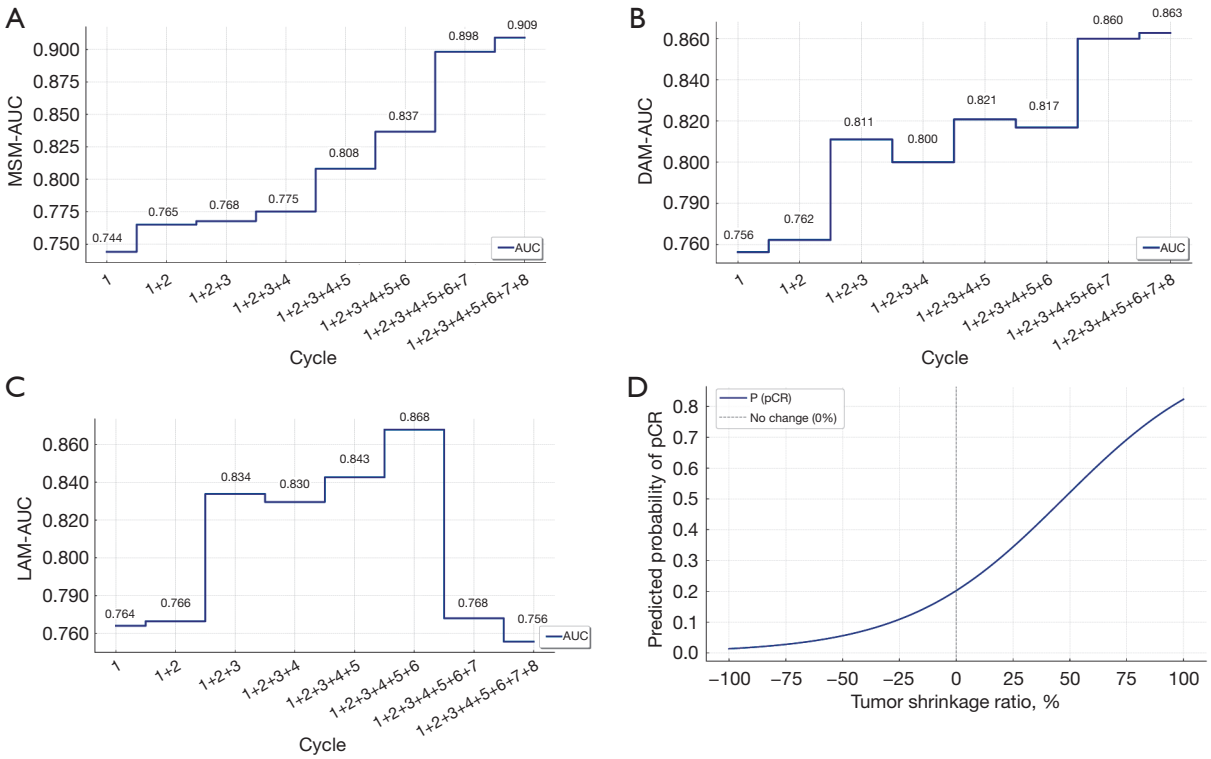

Figure 6 Combined ROC curves and the tumor shrinkage-based pCR prediction curve. (A-C) Combined ROC curves for the MSM, DAM, and LAM across all NAT cycles. The AUC values represent the average predictive performance of each model over time, with confidence intervals displayed. (D) Logistic regression model depicting the relationship between the tumor shrinkage ratio and the probability of achieving a pCR. AUC, area under the curve; DAM, dual axes model; LAM, longest axis model; MSM, manual segment model; NAT, neoadjuvant therapy; pCR, pathologic complete response; ROC, receiver operating characteristic.

and clinicopathological data into a model, and found that tumor diameter reduction after the first cycle of NAT, HER2 status, and posterior acoustic features were independent predictors of the pCR (AUC: 0.912). Unlike previous studies, our research not only confirmed the predictive value of an early response but also introduced a quantitative approach for pCR probability estimation, offering a more objective tool for clinical decision making.

Comparisons across models revealed no statistically significant differences in the AUC values ($P>0.05$), suggesting that the LAM, DAM, and MSM perform similarly in pCR prediction. Compared to our earlier studies (37), this research expanded the sample size and optimized the calculation methods. However, the MSM showed a more stable predictive performance over multiple treatment cycles (*Figure 6A-6C*), particularly in later cycles when tumor shrinkage patterns became more complex. Conversely, the DAM revealed an unexpected increase in tumor size for non-pCR patients after cycle 4, which might be due to its reliance on the product of two diameters. This approach amplifies small measurement variations, making it particularly sensitive to irregular tumor shrinkage patterns (32). Additionally, non-pCR tumors often develop heterogeneous structures, including necrotic cores or fragmented regions, which could affect measurement consistency (38). Moreover, inflammatory responses or treatment-induced edema could temporarily alter tumor morphology, creating an apparent increase in size despite ongoing shrinkage (39). Similarly, the LAM showed a diminishing ability to differentiate between the pCR and non-pCR groups in later cycles (*Figure 3B*). This is likely due to its reliance on a single-axis measurement, which might not accurately reflect true tumor size and shrinkage patterns. Tumors with non-concentric shrinkage, such as those transitioning from a spherical to an elliptical shape or fragmenting into smaller nodules, may not exhibit significant changes in the longest diameter, even when substantial shrinkage has occurred (23). Therefore, the MSM, which considers the tumor's total area, not only better maintained

differentiation between the two groups throughout treatment but also was shown to be a more reliable predictor in early cycles, when clinical decisions regarding treatment adjustments are most impactful (37,40). These findings highlight the importance of using more comprehensive measurement models, particularly in capturing complex tumor responses during later stages of NAT (37).

The limitations of this study include its single-center design and the homogeneity of the patient cohort. Additionally, variations in ultrasound operator experience might have introduced variability in predictive accuracy. Future research should focus on multi-center studies involving more diverse patient populations, and explore integrating ultrasound with other imaging modalities, such as MRI, to potentially enhance the accuracy of pCR predictions. Incorporating additional biomarkers or functional imaging parameters could also enhance the clinical applicability of shrinkage-based predictive models.

Conclusions

This study showed the clinical utility of early cycle ultrasound in predicting the pCR in breast cancer patients undergoing NAT. The ability to quantify tumor shrinkage and estimate the probability of pCR using first-cycle ultrasound measurements provides an objective approach for guiding treatment decisions. For patients exhibiting a poor initial tumor response, early intervention strategies (e.g., treatment regimen adjustments, MRI supplementation, or alternative therapies) may improve outcomes. By optimizing NAT strategies based on the early treatment response, unnecessary toxicity could be minimized, therapeutic efficacy enhanced, and overall patient outcomes improved.

Acknowledgments

None.

Footnote

Reporting Checklist: The authors have completed the TRIPOD + AI reporting checklist (available at https://qims.amegroups.com/article/view/10.21037/qims-24-1444/rc).

Funding: This work was supported in part by the Hubei Provincial Science and Technology Program Project (No. 2023BCB022), the Hubei Provincial Scientific Research Project (No. WJ2023F025), and the Interdisciplinary Innovative Talents Foundation from Renmin Hospital of Wuhan University (No. JCRCYR-2022-014). The funding was used for technical support, software purchases, and text editing.

Conflicts of Interest: All authors have completed the ICMJE uniform disclosure form (available at https://qims.amegroups.com/article/view/10.21037/qims-24-1444/coif). The authors have no conflicts of interest to declare.

Ethical Statement: The authors are accountable for all aspects of the work in ensuring that questions related to the accuracy or integrity of any part of the work are appropriately investigated and resolved. The study was conducted in accordance with the Declaration of Helsinki (as revised in 2013). The study was approved by the Ethics Committee of Renmin Hospital of Wuhan University (approval No. WDRY2022-K217), and informed consent was obtained from all individual participants.

References

1. Bray F, Laversanne M, Sung H, Ferlay J, Siegel RL, Soerjomataram I, Jemal A. Global cancer statistics 2022: GLOBOCAN estimates of incidence and mortality worldwide for 36 cancers in 185 countries. CA Cancer J Clin 2024;74:229-63.
2. Aebi S, Karlsson P, Wapnir IL. Locally advanced breast cancer. Breast 2022;62 Suppl 1:S58-62.
3. Colomer R, Saura C, Sánchez-Rovira P, Pascual T, Rubio IT, Burgués O, Marcos L, Rodríguez CA, Martín M, Lluch A. Neoadjuvant Management of Early Breast Cancer: A Clinical and Investigational Position Statement. Oncologist 2019;24:603-11.
4. Lin YY, Gao HF, Yang X, Zhu T, Zheng XX, Ji F, Zhang LL, Yang CQ, Yang M, Li JQ, Cheng MY, Wang K. Neoadjuvant therapy in triple-negative breast cancer: A systematic review and network meta-analysis. Breast

2022;66:126-35.
5. Korde LA, Somerfield MR, Carey LA, Crews JR, Denduluri N, Hwang ES, Khan SA, Loibl S, Morris EA, Perez A, Regan MM, Spears PA, Sudheendra PK, Symmans WF, Yung RL, Harvey BE, Hershman DL. Neoadjuvant Chemotherapy, Endocrine Therapy, and Targeted Therapy for Breast Cancer: ASCO Guideline. J Clin Oncol 2021;39:1485-505.
6. Ploumen RAW, de Mooij CM, Gommers S, Keymeulen KBMI, Smidt ML, van Nijnatten TJA. Imaging findings for response evaluation of ductal carcinoma in situ in breast cancer patients treated with neoadjuvant systemic therapy: a systematic review and meta-analysis. Eur Radiol 2023;33:5423-35.
7. Yan S, Wang W, Zhu B, Pan X, Wu X, Tao W. Construction of Nomograms for Predicting Pathological Complete Response and Tumor Shrinkage Size in Breast Cancer. Cancer Manag Res 2020;12:8313-23.
8. Baron P, Beitsch P, Boselli D, Symanowski J, Pellicane JV, Beatty J, Richards P, Mislowsky A, Nash C, Lee LA, Murray M, de Snoo FA, Stork-Sloots L, Gittleman M, Akbari S, Whitworth P. Impact of Tumor Size on Probability of Pathologic Complete Response After Neoadjuvant Chemotherapy. Ann Surg Oncol 2016;23:1522-9.
9. von Minckwitz G, Untch M, Blohmer JU, Costa SD, Eidtmann H, Fasching PA, Gerber B, Eiermann W, Hilfrich J, Huober J, Jackisch C, Kaufmann M, Konecny GE, Denkert C, Nekljudova V, Mehta K, Loibl S. Definition and impact of pathologic complete response on prognosis after neoadjuvant chemotherapy in various intrinsic breast cancer subtypes. J Clin Oncol 2012;30:1796-804.
10. Yau C, Osdoit M, van der Noordaa M, Shad S, Wei J, de Croze D, et al. Residual cancer burden after neoadjuvant chemotherapy and long-term survival outcomes in breast cancer: a multicentre pooled analysis of 5161 patients. Lancet Oncol 2022;23:149-60.
11. Spring L, Greenup R, Niemierko A, Schapira L, Haddad S, Jimenez R, Coopey S, Taghian A, Hughes KS, Isakoff SJ, Ellisen LW, Smith BL, Specht M, Moy B, Bardia A. Pathologic Complete Response After Neoadjuvant Chemotherapy and Long-Term Outcomes Among Young Women With Breast Cancer. J Natl Compr Canc Netw 2017;15:1216-23.
12. Rubio IT, Sobrido C. Neoadjuvant approach in patients with early breast cancer: patient assessment, staging, and planning. Breast 2022;62 Suppl 1:S17-24.
13. Huang YH, Shi ZY, Zhu T, Zhou TH, Li Y, Li W, Qiu H, Wang SQ, He LF, Wu ZY, Lin Y, Wang Q, Gu WC, Gu CC, Song XY, Zhou Y, Guan DG, Wang K. Longitudinal MRI-Driven Multi-Modality Approach for Predicting Pathological Complete Response and B Cell Infiltration in Breast Cancer. Adv Sci (Weinh) 2025. [Epub ahead of print]. doi: 10.1002/advs.202413702.
14. Zhang C, Kosiorek HE, Patel BK, Pockaj BA, Ahmad SB, Cronin PA. Accuracy of Posttreatment Imaging for Evaluation of Residual in Breast Disease After Neoadjuvant Endocrine Therapy. Ann Surg Oncol 2022;29:6207-12.
15. Reig B, Heacock L, Lewin A, Cho N, Moy L. Role of MRI to Assess Response to Neoadjuvant Therapy for Breast Cancer. J Magn Reson Imaging 2020.
16. Marinovich ML, Houssami N, Macaskill P, Sardanelli F, Irwig L, Mamounas EP, von Minckwitz G, Brennan ME, Ciatto S. Meta-analysis of magnetic resonance imaging in detecting residual breast cancer after neoadjuvant therapy. J Natl Cancer Inst 2013;105:321-33.
17. Li JJ, Chen C, Gu Y, Di G, Wu J, Liu G, Shao Z. The role of mammographic calcification in the neoadjuvant therapy of breast cancer imaging evaluation. PLoS One 2014;9:e88853.
18. Iotti V, Ragazzi M, Besutti G, Marchesi V, Ravaioli S, Falco G, Coiro S, Bisagni A, Gasparini E, Giorgi Rossi P, Vacondio R, Pattacini P. Accuracy and Reproducibility of Contrast-Enhanced Mammography in the Assessment of Response to Neoadjuvant Chemotherapy in Breast Cancer Patients with Calcifications in the Tumor Bed. Diagnostics (Basel) 2021;11:435.
19. Chong A, Weinstein SP, McDonald ES, Conant EF. Digital Breast Tomosynthesis: Concepts and Clinical Practice. Radiology 2019;292:1-14.
20. Kaplan SS. Automated whole breast ultrasound. Radiol Clin North Am 2014;52:539-46.
21. Covington MF, Parent EE, Dibble EH, Rauch GM, Fowler AM. Advances and Future Directions in Molecular Breast Imaging. J Nucl Med 2022;63:17-21.
22. Le EPV, Wang Y, Huang Y, Hickman S, Gilbert FJ. Artificial intelligence in breast imaging. Clin Radiol 2019;74:357-66.
23. Lim HF, Sharma A, Gallagher C, Hall P. Value of ultrasound in assessing response to neoadjuvant chemotherapy in breast cancer. Clin Radiol 2023;78:912-8.
24. El-Diasty MT, Ageely GA, Sawan S, Karsou RM, Bakhsh SI, Alharthy A, Noorelahi Y, Badeeb A. The Role of Ultrasound Features in Predicting the Breast Cancer Response to Neoadjuvant Chemotherapy. Cureus

2023;15:e49084.
25. Sabeti S, Larson NB, Boughey JC, Stan DL, Solanki MH, Fazzio RT, Fatemi M, Alizad A. Ultrasound-based quantitative microvasculature imaging for early prediction of response to neoadjuvant chemotherapy in patients with breast cancer. Breast Cancer Res 2025;27:24.
26. Gradishar WJ, Anderson BO, Abraham J, Aft R, Agnese D, Allison KH, et al. Breast Cancer, Version 3.2020, NCCN Clinical Practice Guidelines in Oncology. J Natl Compr Canc Netw 2020;18:452-78.
27. Gradishar WJ, Moran MS, Abraham J, Aft R, Agnese D, Allison KH, , et al. Breast Cancer, Version 3.2022, NCCN Clinical Practice Guidelines in Oncology. J Natl Compr Canc Netw 2022;20:691-722.
28. Jiang Z, Song E, Wang X, et al. Guidelines of Chinese Society of Clinical Oncology (CSCO) on Diagnosis and Treatment of Breast Cancer (2020 version). Transl Breast Cancer Res 2020;1:27.
29. Jiang Z, Li J, Chen J, Liu Y, Wang K, Nie J, Wang X, Hao C, Yin Y, Wang S, Yan M, Wang T, Yan Y, Chen X, Song E; CSCO BC guideline working group. Chinese Society of Clinical Oncology (CSCO) Breast Cancer Guidelines 2022. Transl Breast Cancer Res 2022;3:13.
30. Nahleh Z, Sivasubramaniam D, Dhaliwal S, Sundarajan V, Komrokji R. Residual cancer burden in locally advanced breast cancer: a superior tool. Curr Oncol 2008;15:271-8.
31. Viale G, Fusco N. Pathology after neoadjuvant treatment - How to assess residual disease. Breast 2022;62 Suppl 1:S25-8.
32. Eisenhauer EA, Therasse P, Bogaerts J, Schwartz LH, Sargent D, Ford R, Dancey J, Arbuck S, Gwyther S, Mooney M, Rubinstein L, Shankar L, Dodd L, Kaplan R, Lacombe D, Verweij J. New response evaluation criteria in solid tumours: revised RECIST guideline (version 1.1). Eur J Cancer 2009;45:228-47.
33. Wang KN, Meng YJ, Yu Y, Cai WR, Wang X, Cao XC, Ge J. Predicting pathological complete response after neoadjuvant chemotherapy: A nomogram combining clinical features and ultrasound semantics in patients with invasive breast cancer. Front Oncol 2023;13:1117538.
34. Bruno R, Bottino D, de Alwis DP, Fojo AT, Guedj J, Liu C, Swanson KR, Zheng J, Zheng Y, Jin JY. Progress and Opportunities to Advance Clinical Cancer Therapeutics Using Tumor Dynamic Models. Clin Cancer Res 2020;26:1787-95.
35. Duan Y, Song X, Guan L, Wang W, Song B, Kang Y, Jia Y, Zhu Y, Nie F. Comparative study of pathological response evaluation systems after neoadjuvant chemotherapy for breast cancer: developing predictive models of multimodal ultrasound features including shear wave elastography combined with puncture pathology. Quant Imaging Med Surg 2023;13:3013-28.
36. Wen X, Chen J, Zhong J, Zhuang Y, Deng B, Lin Y, Su Z. Model based on ultrasound and clinicopathological characteristics for early prediction of pathological complete response to neoadjuvant chemotherapy in breast cancer. Quant Imaging Med Surg 2024;14:8840-51.
37. Zhang J, Deng J, Huang J, Mei L, Liao N, Yao F, Lei C, Sun S, Zhang Y. Monitoring response to neoadjuvant therapy for breast cancer in all treatment phases using an ultrasound deep learning model. Front Oncol 2024;14:1255618.
38. Gillies RJ, Anderson AR, Gatenby RA, Morse DL. The biology underlying molecular imaging in oncology: from genome to anatome and back again. Clin Radiol 2010;65:517-21.
39. Hygino da Cruz LC Jr, Rodriguez I, Domingues RC, Gasparetto EL, Sorensen AG. Pseudoprogression and pseudoresponse: imaging challenges in the assessment of posttreatment glioma. AJNR Am J Neuroradiol 2011;32:1978-85.
40. Gounaris I, Provenzano E, Vallier AL, Hiller L, Iddawela M, Hilborne S, Taylor K, Britton P, Earl HM, Sinnatamby R. Accuracy of unidimensional and volumetric ultrasound measurements in predicting good pathological response to neoadjuvant chemotherapy in breast cancer patients. Breast Cancer Res Treat 2011;127:459-69.

Cite this article as: Deng J, Liao S, Wang L, Zhang J, Jia Y, Yao F, Sun S, Zhang Y. Investigating the optimal timing for the ultrasound prediction of a pathologic complete response in neoadjuvant breast cancer treatment. Quant Imaging Med Surg 2025;15(4):3616-3630. doi: 10.21037/qims-24-1444